Supplementary Information (SI) for Journal of Materials Chemistry A.
This journal is © The Royal Society of Chemistry 2026

Supporting Information

Linkage-Enabled π-Conjugation Engineering in an Oxime-Based Nickel Covalent Organic Framework Unlocks Efficient Oxygen Activation

*Dekang Huang[a], Xiaodong Zhao[a], Huaji Pang[a], Hongyu Chen[a], Yunxiang Li[b], Dingtang Li[c], Lin Gao[d], Ming Lei[e], Lijuan Fu[a], Yonggang Xiang[a]**

[a]Hubei Key Laboratory of Agricultural Functional Materials, College of Chemistry, Huazhong Agricultural University, Wuhan 430070, PR China

[b]Engineering Research Center of Photoenergy Utilization for Pollution Control and Carbon Reduction, Ministry of Education, College of Chemistry, Central China Normal University, Wuhan 430079, PR China

[c]State Key Laboratory of Agricultural Microbiology Core Facility, Huazhong Agricultural University, Wuhan 430070, PR China

[d]Hubei Key Laboratory of Energy Storage and Power Battery, School of Optoelectronic Engineering, School of New Energy, Hubei University of Automotive Technology, Shiyan 442002, PR China

[e]College of Resources and Environmental Science, South-Central Minzu University, Wuhan 430074, PR China

E-mail: ygxiang@mail.hzau.edu.cn (Y. Xiang)

Table of Contents

1. General information

1.1 Chemicals

Unless otherwise noted, all the chemicals were purchased in analytical purity from commercial suppliers and used directly without further purification.

1.2 Characterization methods

Powder X-ray diffraction (PXRD) patterns were collected on a Bruker D8 Advance diffractometer with Cu Kα radiation (2θ range: 2-30°; Scan step size: 0.02°; Time per step: 1 s). Liquid-state ^{1}H NMR and ^{13}C NMR were recorded on Bruker Advance 600 MHz and 150 MHz spectrometers at 298 K, respectively, and chemical shift (δ) was reported in ppm with residual solvent peak as the reference. Peaks are reported as follows: s = singlet, d = doublet, t = triplet, q = quartet, m = multiplet or unresolved, with coupling constants in Hz. Fourier transform infrared (FT-IR) spectra were collected on a Nicolet 6700 spectrometer (Thermo Scientific, USA) equipped with an ATR cell. In situ diffuse reflectance infrared Fourier transform spectroscopy (DRIFTS) measurements were performed using a Bruker INVENIO S Fourier Transform Infrared Spectrometer equipped with a Harrick diffuse reflectance accessory. The specific Brunauer-Emmett-Teller (BET) surface area and pore size distribution were measured using a BSD-PM1 instrument at 77 K. High resolution transmission electron microscope (HRTEM) images were obtained on a JEOL JEM-F200 instrument. Scanning electron microscopy (SEM) images were collected using a Hitachi SU 8010 microscope. Solid-state ^{13}C cross polarization magic angle spinning (^{13}C-CP/MAS) NMR spectra were collected on a Bruker Avance III HD 400 spectrometer. X-ray photoelectron spectroscopy (XPS) measurements were performed

on a Thermo ESCALAB 250 spectrometer with C 1s (284.6 eV) as the reference line. Solid-state diffuse reflectance UV-vis spectra were collected on a Shimadzu UV 3600 spectrophotometer with $BaSO_4$ as the reference. The generation of reactive oxygen species (ROS) was determined by electron spin resonance (ESR) spectra, which were recorded on a EPR200-Plus spectrometer. The concentrations of CIP were quantified by a high-performance liquid chromatography (HPLC) (Alliance e2695). The intermediate products were resolved by a high-resolution mass spectrometer (HRMS, Thermo Scientific Q Exactive). X-ray absorption spectroscopy (XAS) measurements were conducted a TableXAFS-500 apparatus (Anhui Chuangpu Instrument Technology Co., Ltd.). Ni leaching was tested by inductively coupled plasma mass spectrometry (ICP-MS, Agilent 5800 ICP-OES).

1.3 Electrochemical measurements

Electrochemical measurements were performed on a CHI760E workstation (Chenhua Instruments, China), and the standard three-electrode system included a platinum plate as the counter electrode, a commercial Ag/AgCl electrode as the reference electrode, and a working electrode. The working electrode was prepared as follows: 15 mg of sample was thoroughly mixed with 200 μL isopropanol containing 5% Nafion, and the resulting suspension was carefully loaded on the ITO glass substrate and dried at 60 ^{o}C under vacuum for 1 h. 0.1 M Na_2SO_4 aqueous solution was employed as the electrolyte for the photocurrent test while the aqueous solution containing 0.1 M KCl and 0.005 M $K_3[Fe(CN)_6]$ was employed as the electrolyte for the electrochemical impedance spectroscopy (EIS) measurement. For Mott-Schottky

tests, the perturbation was 5 mV with frequencies of 1000, 2000, and 3000 Hz.

The open-circuit potential (OCP) decay following light-off reflects the surface charge recombination dynamics of trapped carriers. The average surface recombination rate can be obtained by fitting the decay curve with a first-order kinetic model.

$$\frac{E - E_{ph}}{E_0 - E_{ph}} = 1 - \exp\left(-K_r t\right)$$

where E is the open-circuit potential at any time, E_0 is the stationary OCP value in the dark, E_{ph} is the photostationary OCP value, and k_r is the pseudo-first-order recombination rate constant.

1.4 Photocatalytic oxidation of TMB

25 mg of 3,3',5,5'-tetramethylbenzidine (TMB) was dissolved in 2.5 mL of ethanol. 200 μL of TMB solution and 7 mg of COFs were added into 0.1 M HAc/NaAc buffer solution (20 mL, pH 4). After saturation of adsorption, the photocatalytic oxidation of TMB was carried out under the irradiation of a 300 W xenon lamp (λ > 420 nm, PLS SXE300, Beijing Perfectlight Technology Co., Ltd.). TMB oxidation were evaluated by UV–vis measurements (the absorbance at 369 nm) at different time intervals.

1.5 Photocatalytic degradation of ciprofloxacin

The photocatalytic experiments were carried out using a 300 W xenon lamp (λ > 420 nm, PLS SXE300, Beijing Perfectlight Technology Co., Ltd.). 10 mg of COFs were dispersed in 10 mL of 50 mg L^{-1} CIP aqueous solution by ultrasonication for 5 minutes to ensure uniform dispersion of the photocatalyst. The suspension was then stirred in the dark for 60 minutes to establish adsorption–desorption equilibrium. Subsequently,

photocatalytic reactions were conducted under xenon lamp irradiation for another 60 minutes, with 500 μL aliquots collected every 15 minutes. Throughout the experiment, the system was maintained under an oxygen atmosphere. The collected samples were filtered through a nylon syringe filter with a pore size of 0.22 μm and then injected into HPLC vials for analysis. The degradation efficiency of ciprofloxacin was calculated according to the following equation.

$$\text{Degradation efficiency}\,(\%) = (1 - \frac{C_t}{C_0}) \times 100\%$$

Where C_0 represents the concentration of CIP after reaching adsorption-desorption equilibrium following 60 minutes of dark treatment, while C_t denotes the residual concentration of CIP at a given irradiation time.

The photocatalytic degradation of CIP follows first-order reaction kinetics, which can be described by the following equation:

$$\ln\frac{C_t}{C_0} = kt$$

Where k is the apparent reaction rate constant and t is the reaction time.

2. Synthetic procedures

2.1 Synthesis of small molecules

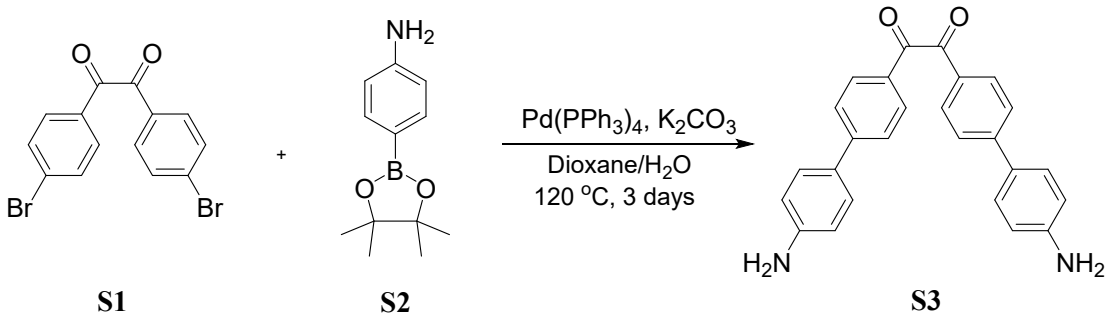

S1 **S2** **S3**

Scheme S1. Synthesis of **S3**.

Synthesis of S3: A mixture of 4,4'-dibromobenzil (**S1**, 2.0 g, 5.4 mmol), 4-aminophenylboronic acid pinacol ester (**S2**, 5.8 g, 26.5 mmol), $Pd(PPh_3)_4$ (0.12 g, 0.1 mmol), and K_2CO_3 (4.2 g, 30.4 mmol) in a solvent system of 1,4-dioxane (52 mL) and distilled water (14 mL) was placed in a round-bottom flask. The reaction mixture was stirred at 120 °C under an argon atmosphere for 3 days. After completion of the reaction, the mixture was cooled to room temperature and concentrated under reduced pressure to afford a solid residue. The crude product was successively washed with deionized water and methanol, followed by vacuum drying at 60 °C for 12 h to yield the target compound **S3**. ^{1}H NMR (DMSO-d_6, 600 MHz) δ 7.89 (d, J = 8.4 Hz, 4H), 7.81 (d, J = 8.4 Hz, 4H), 7.51 (d, J = 8.4 Hz, 4H), 6.67 (d, J = 7.8 Hz, 4H), 5.55 (s, 4H). ^{13}C NMR (151 MHz, DMSO-d_6) δ 194.47, 150.16, 147.32, 130.33, 129.41, 128.06, 125.60, 124.89, 114.21.

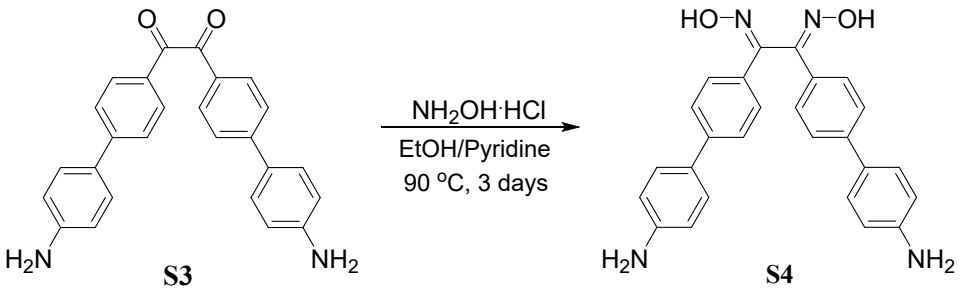

Scheme S2. Synthesis of **S4**.

Synthesis of S4: S3 (1.0 g, 2.55 mmol), hydroxylamine hydrochloride ($NH_2OH·HCl$, 1.76 g, 25.5 mmol), and a mixed solvent of pyridine (20 mL) and anhydrous ethanol (30 mL) were added to a round-bottom flask. The mixture was degassed with Ar for 10 min and then stirred at 90 °C under an Ar atmosphere for 3 days. After cooling to room temperature, the reaction was quenched by water (200 mL). The resulting suspension was filtered to afford a pale yellow precipitate **S4** (1.06 g, 2.5 mmol, 98%). ^{1}H NMR (DMSO-d_6, 600 MHz) δ 11.34 (s, 2H), 7.54 (d, J = 8.4 Hz, 4H), 7.49 (d, J = 8.4 Hz, 4H), 7.35 (d, J = 8.4 Hz, 4H), 6.61 (d, J = 8.4 Hz, 4H), 5.27 (s, 4H). ^{13}C NMR (151 MHz, DMSO-d_6) δ 151.18, 149.22, 141.96, 136.61, 130.54, 127.63, 126.97, 126.48, 114.62.

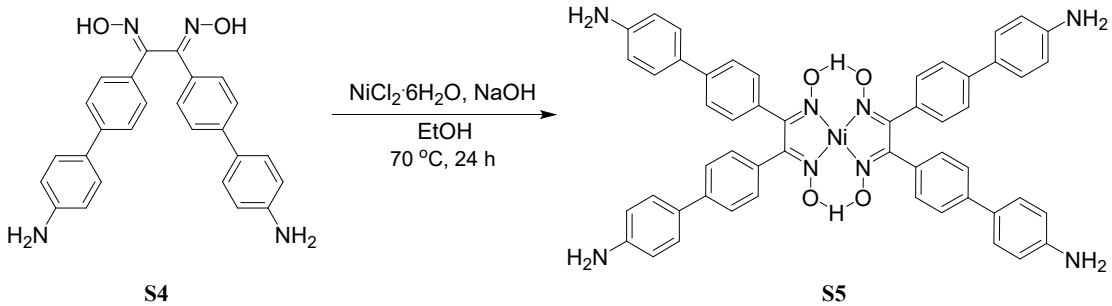

Scheme S3. Synthesis of **S5**.

Synthesis of S5: S4 (0.5 g, 1.18 mmol) and sodium hydroxide (NaOH, 0.4 g, 10 mmol) were dissolved in anhydrous ethanol (50 mL) in a round-bottom flask and stirred for 10 min. A solution of nickel(II) chloride hexahydrate ($NiCl_2·6H_2O$, 0.14 g, 0.6 mmol) in

anhydrous ethanol (5 mL) was slowly added to the mixture. After degassing with Ar for 10 min, the reaction was stirred at 70 °C under an Ar atmosphere for 24 h. Upon cooling, the suspension was filtered to afford a brown precipitate **S5** (0.31 g, 0.34 mmol, 57%). ^{1}H NMR (DMSO-d_6, 600 MHz) δ 7.54 (d, J = 8.4 Hz, 8H), 7.48 (d, J = 8.4 Hz, 8H), 7.35 (d, J = 8.4 Hz, 8H), 6.61 (d, J = 8.4 Hz, 8H), 5.26 (s, 8H). ^{13}C NMR spectra of **S5** can not be obtained because of its insufficient solubility in organic solvents. MS (HR-ESI): m/z Calc. $C_{52}H_{43}N_8O_4Ni$ $[M+H]^+$ 901.2761, found 901.2764.

2.2 Synthesis of I-Ni-COF

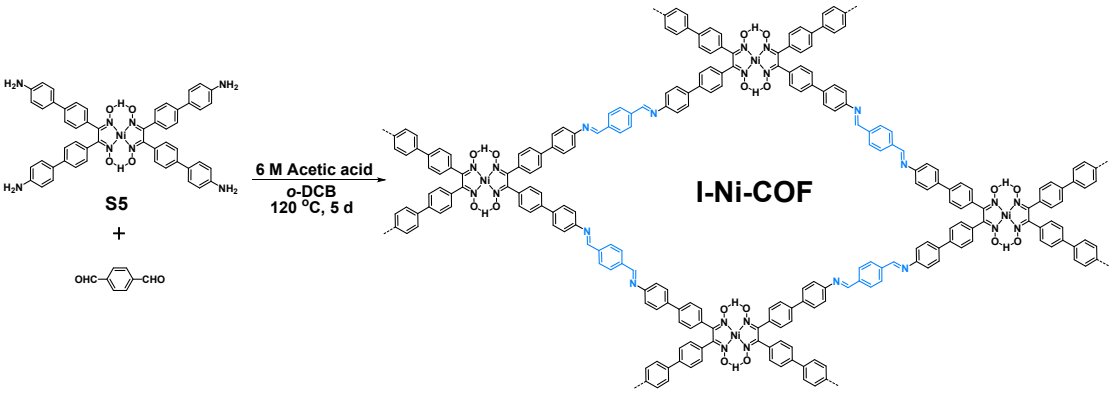

Scheme S4. Synthesis of **I-Ni-COF**.

A glass tube (10 mL) was charged with **S5** (27.1 mg, 0.03 mmol), terephthalaldehyde (11.3 mg, 0.06 mmol), 1,2-dichlorobenzene (1 mL), and HOAc (6 mol L^{-1}, 0.2 mL). Subsequently, the tube was sonicated for 10 minutes, degassed by three freeze-pump-thaw cycles (liquid nitrogen), and sealed under vacuum. After being heated in an oven at 120 °C for 5 days, the cooled suspension was centrifuged to separate the solid, which was repeatedly washed by THF and CH_3OH until the supernatant became colorless. **I-Ni-COF** was obtained as a green powder (33.6 mg) after being dried under vacuum at 80 °C.

2.3 Synthesis of NQ-Ni-COF

I-Ni-COF (50 mg), ethylene carbonate (40 mg, 0.46 mmol), $[Cp^*RhCl_2]_2$ (5 mg, 0.0075 mmol), and i-PrOH (2.5 mL) were placed in a Pyrex glass tube (10 mL). The mixture was ultrasonicated for 5 min, degassed via three freeze-pump-thaw cycles (liquid nitrogen), and sealed under vacuum. The mixture was reacted at 110 °C for 12 h. After cooling to room temperature, the solid product was isolated by filtration under reduced pressure and sequentially washed with water and CH_3OH. **NQ-Ni-COF** was obtained as a brown powder (30.5 mg) after dried under vacuum at 80 °C.

3. Characterization

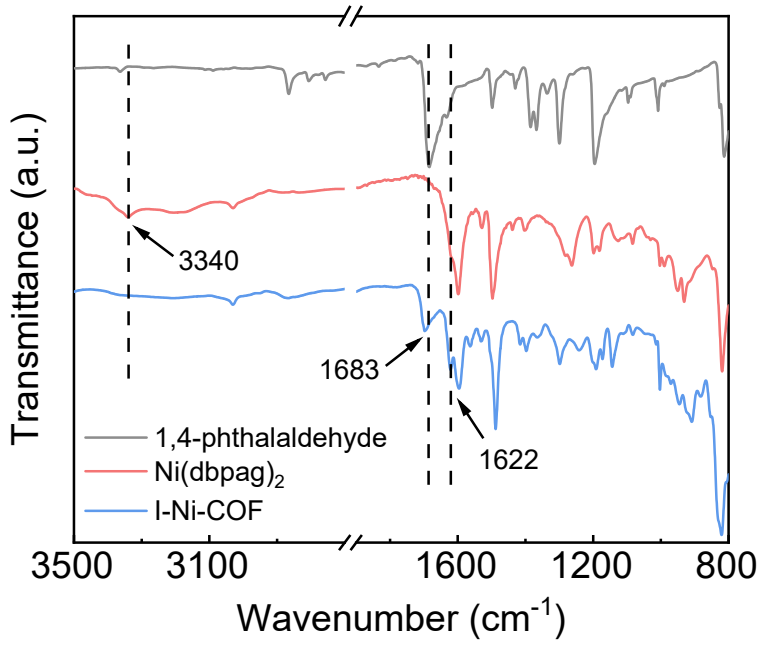

Fig. S1 FT-IR spectra of 1,4-phthalaldehyde, $Ni(dbpag)_2$, and I-Ni-COF.

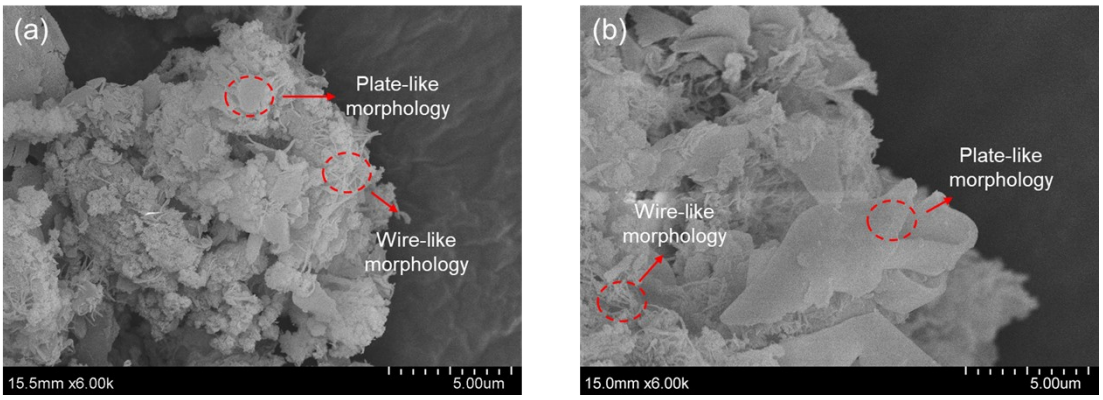

Fig. S2 SEM images of (a) I-Ni-COF and (b) NQ-Ni-COF.

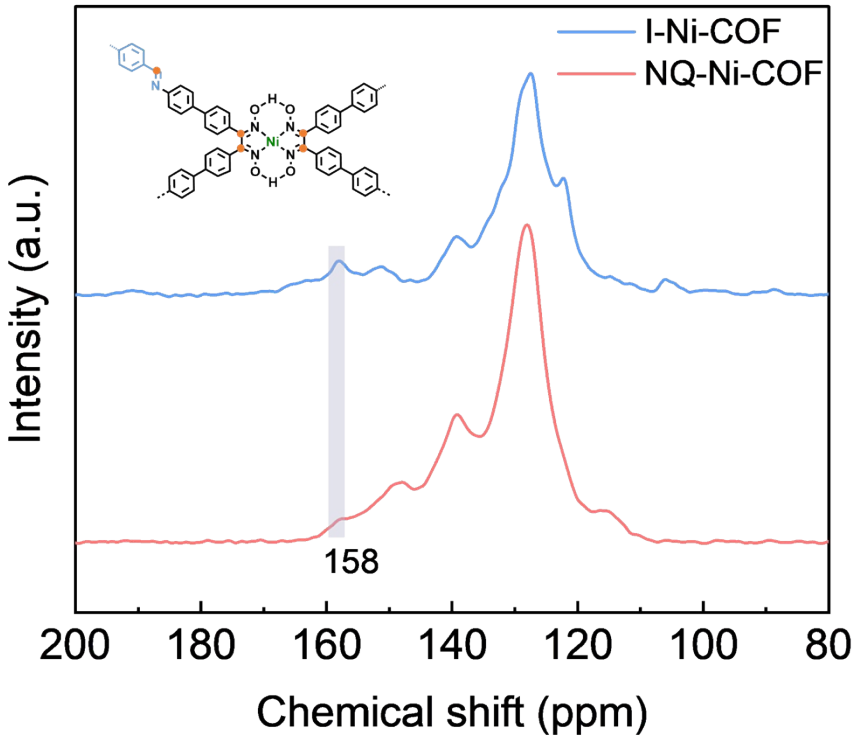

Fig. S3 ^{13}C CP-MAS NMR spectra of I-Ni-COF and NQ-Ni-COF. The signal at 158 ppm in I-Ni-COF is ascribed to the imine carbon and oxime carbon.

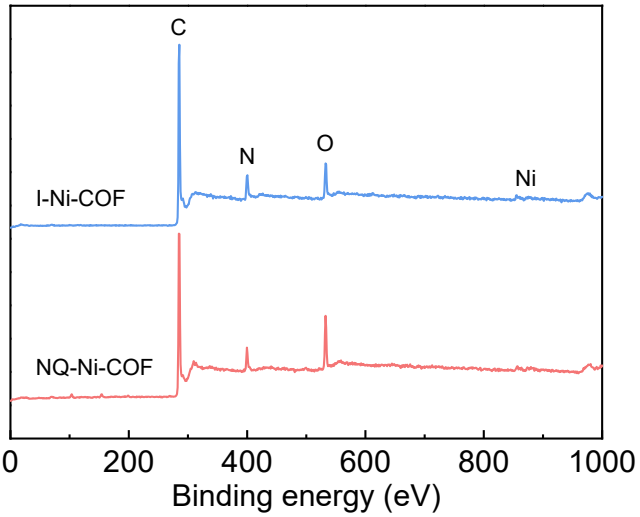

Fig. S4 XPS survey spectra of I-Ni-COF and NQ-Ni-COF.

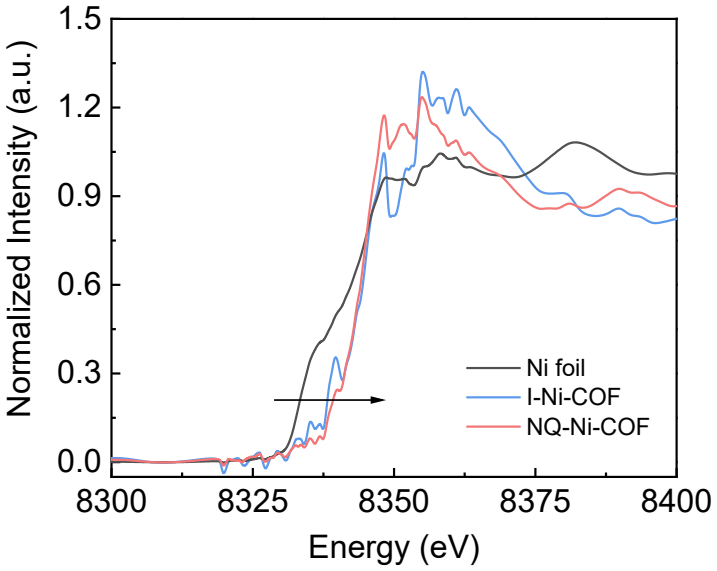

Fig. S5 Ni K-edge XANES spectra of Ni foil, I-Ni-COF, and NQ-Ni-COF.

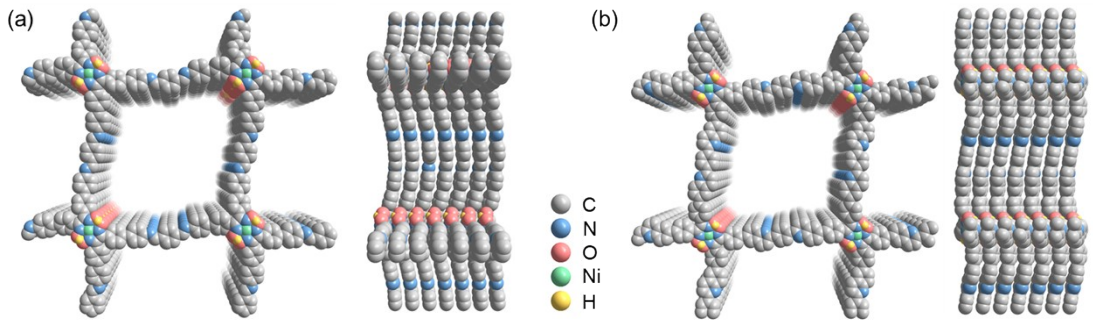

Fig. S6 Top and side views of the simulated structures of (a) I-Ni-COF and (b) NQ-Ni-COF with the eclipsed AA stacking models.

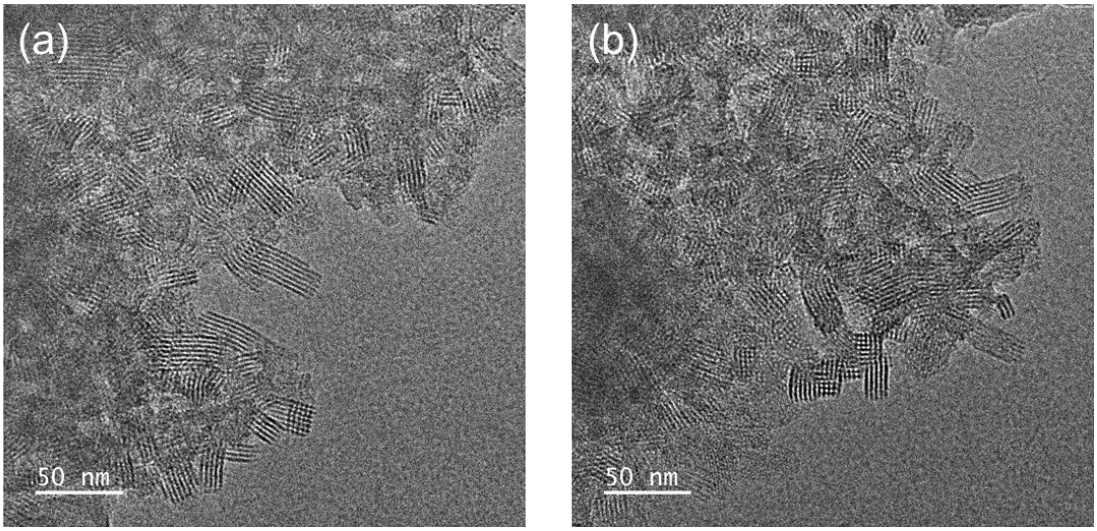

Fig. S7 HRTEM images of I-Ni-COF.

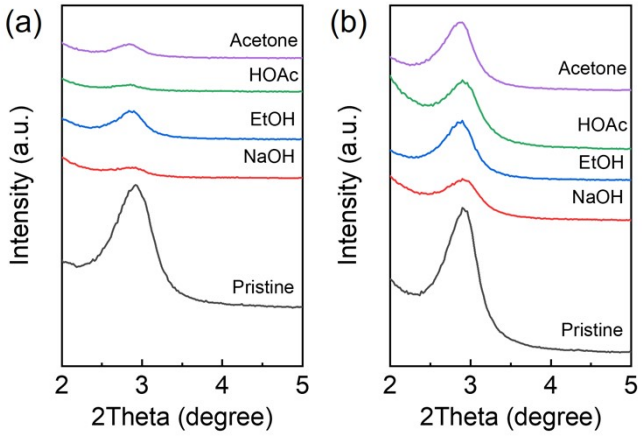

Fig S8. PXRD patterns of I-Ni-COF (a) and NQ-Ni-COF (b) treated in different chemical environments for 12 hours.

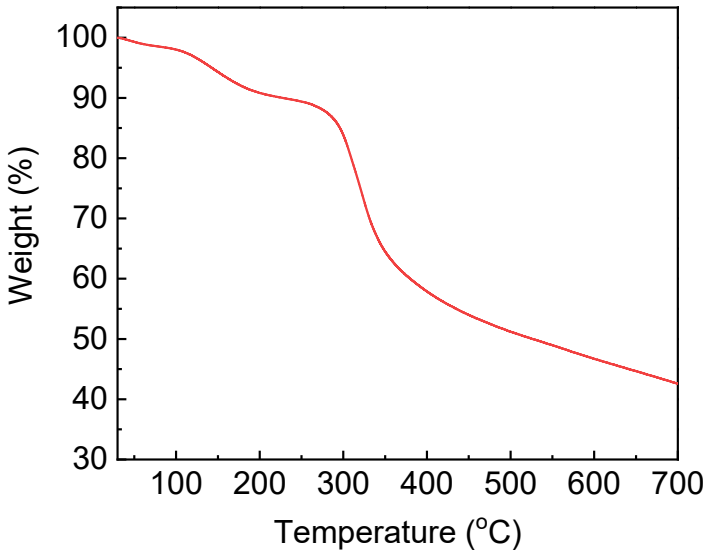

Fig. S9 Thermogravimetric curve of NQ-Ni-COF.

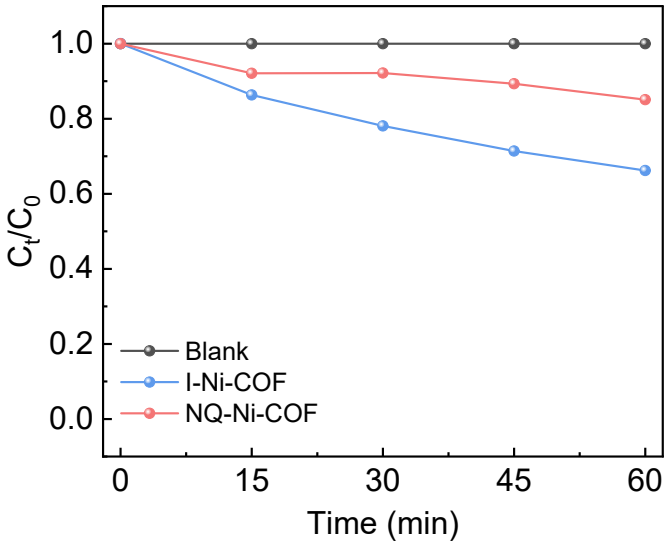

Fig. S10 Adsorption behaviors of I-Ni-COF and NQ-Ni-COF under dark conditions.

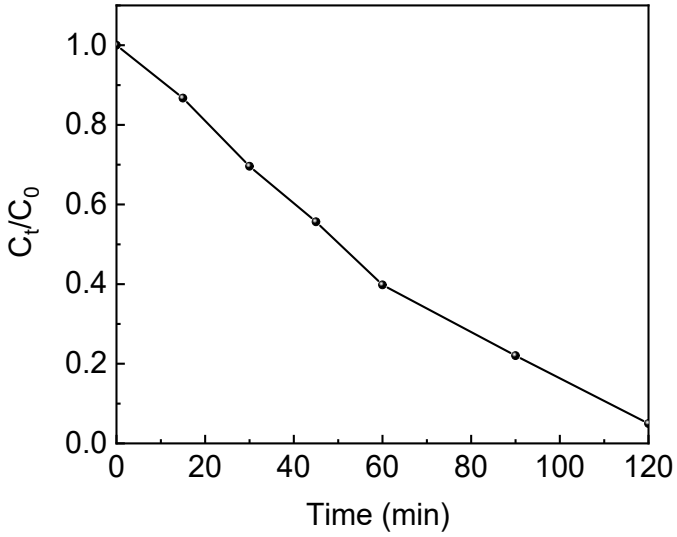

Fig. S11 CIP degradation curve over the NQ-Ni-COF photocatalyst in actual wastewater.

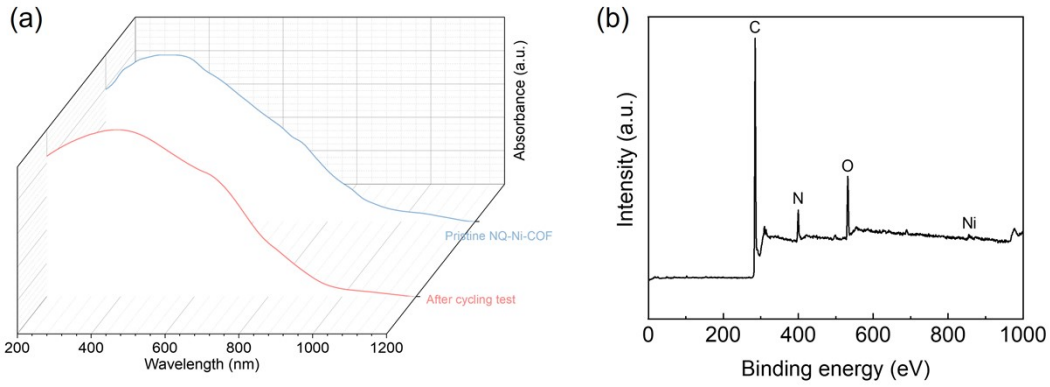

Fig. S12 (a) UV-vis DRS spectra of NQ-Ni-COF before and after cycling test. (b) XPS spectrum of NQ-Ni-COF after cycling test.

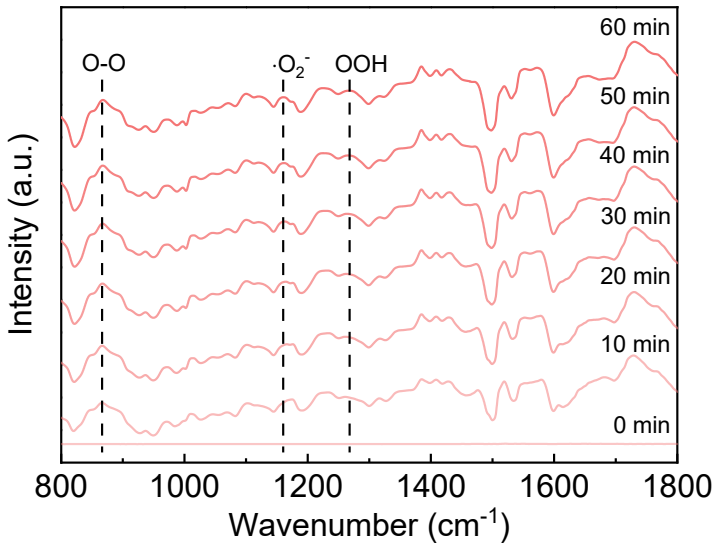

Fig. S13 *In situ* DRIFT spectra recorded during photocatalytic O_2 activation for NQ-Ni-COF.

Table S1. Atomistic coordinates of AA stacking for I-Ni-COF.

Atom	*x/a*	*y/b*	*z/c*
C1	0.56499	0.52321	0.79713
C2	0.58889	0.48783	0.91807
C3	0.63334	0.48734	0.8779
C4	0.65459	0.52279	0.72355
C5	0.63052	0.55786	0.60285
C6	0.58656	0.55793	0.63854
C7	0.70157	0.52493	0.69875
C8	0.51865	0.52789	0.86996
C9	0.48468	0.49301	0.87757
C10	0.48948	0.44639	0.78675
C11	0.45506	0.41889	0.85324
C12	0.45671	0.37559	0.76442
C13	0.49328	0.35781	0.60775
C14	0.52836	0.38475	0.54121
C15	0.52623	0.42874	0.62778
C16	0.49331	0.31155	0.5115
N17	0.50277	0.56575	0.94257
N18	0.44728	0.50879	0.96041
O19	0.40766	0.49035	0.9317
O20	0.52081	0.60583	0.90954
Ni21	0.44637	0.5659	0.9437
H22	0.50302	0.62627	1.12402
H23	0.38784	0.5082	1.14952
N24	0.4456	0.6227	0.89359
N25	0.39006	0.56584	0.91001
C26	0.40887	0.63709	0.77787
C27	0.37487	0.60235	0.7912
C28	0.40479	0.68193	0.63734
C29	0.32932	0.60545	0.68491
C30	0.44139	0.70307	0.51203
C31	0.44045	0.74608	0.41033
C32	0.40262	0.76963	0.43014
C33	0.36542	0.74862	0.54696
C34	0.36663	0.70515	0.64951
C35	0.3033	0.63978	0.79341
C36	0.25905	0.63784	0.74353
C37	0.2401	0.601	0.59118
C38	0.26632	0.56714	0.47831
C39	0.31012	0.56942	0.52459
C40	0.40338	0.81634	0.35048
C41	0.1933	0.59572	0.57352

O42	0.48531	0.64113	0.87767
O43	0.3721	0.52556	0.90569
C44	0.44208	0.83643	0.26305
C45	0.44429	0.88079	0.21543
C46	0.40769	0.90615	0.25364
C47	0.36882	0.88631	0.33412
C48	0.36663	0.8417	0.38256
C49	0.16551	0.62991	0.64993
C50	0.1214	0.62329	0.6529
C51	0.10456	0.58244	0.58268
C52	0.13229	0.5484	0.50291
C53	0.17608	0.55505	0.4981
C54	0.45483	0.28874	0.51882
C55	0.45363	0.24508	0.43878
C56	0.49104	0.22293	0.34897
C57	0.52965	0.24544	0.3383
C58	0.53081	0.28957	0.41801
C59	0.72729	0.48876	0.76193
C60	0.77171	0.49215	0.74173
C61	0.79081	0.53189	0.65993
C62	0.76525	0.56776	0.59806
C63	0.72116	0.56432	0.61648
N64	0.83593	0.53726	0.64086
N65	0.49033	0.17752	0.28125
C66	0.45494	0.15603	0.283
C67	0.45311	0.1094	0.23206
C68	0.41349	0.08916	0.25432
C69	0.4105	0.04447	0.23079
C70	0.44726	0.01963	0.18382
C71	0.48689	0.0399	0.15702
C72	0.4899	0.08467	0.18129
C73	0.44534	-0.02742	0.18424
C74	0.86316	0.50616	0.6646
C75	0.90895	0.51497	0.64499
C76	0.93764	0.48067	0.63884
C77	0.98138	0.48852	0.61858
C78	0.99674	0.53069	0.60583
C79	0.96806	0.56513	0.61285
C80	0.92435	0.55728	0.63164
C81	1.04276	0.53771	0.58628
N82	1.05949	0.5758	0.60148
N83	0.40983	-0.04792	0.23326

Table S2. Atomistic coordinates of AA stacking for NQ-Ni-COF.

Atom	*x/a*	*y/b*	*z/c*
C1	0.5954	0.4894	0.157
C2	0.622	0.4552	0.2631
C3	0.6663	0.4586	0.2297
C4	0.6849	0.4967	0.0931
C5	0.6582	0.5303	-0.0226
C6	0.6142	0.5266	0.0088
C7	0.7316	0.5036	0.1
C8	0.5492	0.4907	0.2458
C9	0.5169	0.4538	0.2463
C10	0.5242	0.4069	0.1809
C11	0.4898	0.3819	0.0582
C12	0.4914	0.337	0.0633
C13	0.528	0.3157	0.1874
C14	0.5634	0.3403	0.2945
C15	0.5613	0.3856	0.2935
C16	0.5264	0.2688	0.2538
N17	0.5311	0.5276	0.3248
N18	0.4789	0.4675	0.3341
O19	0.4415	0.4453	0.3944
O20	0.5478	0.5684	0.3661
Ni21	0.4765	0.5233	0.4343
H22	0.5241	0.5902	0.2077
H23	0.4303	0.4571	0.6804
N24	0.4742	0.579	0.5372
N25	0.422	0.5189	0.5472
C26	0.4366	0.5922	0.6429
C27	0.4043	0.5555	0.6414
C28	0.43	0.6383	0.743
C29	0.3584	0.5568	0.7397
C30	0.4646	0.6615	0.8857
C31	0.4628	0.7061	0.9273
C32	0.4262	0.729	0.8272
C33	0.3908	0.706	0.6954
C34	0.3929	0.661	0.6518
C35	0.3317	0.591	0.6364
C36	0.2874	0.5875	0.6748
C37	0.2691	0.5494	0.8132
C38	0.2959	0.5158	0.9255
C39	0.3399	0.5195	0.889
C40	0.427	0.7769	0.8305
C41	0.2224	0.5425	0.8103

O42	0.512	0.6009	0.4942
O43	0.4057	0.4778	0.5219
C44	0.466	0.7984	0.8755
C45	0.4684	0.8432	0.8496
C46	0.4314	0.8676	0.7785
C47	0.3923	0.8465	0.7383
C48	0.3902	0.8013	0.7625
C49	0.1942	0.5754	0.7022
C50	0.1506	0.5669	0.6702
C51	0.1348	0.5251	0.743
C52	0.1626	0.4926	0.856
C53	0.2059	0.5013	0.889
C54	0.4871	0.2494	0.3354
C55	0.4842	0.2051	0.3939
C56	0.5209	0.179	0.3709
C57	0.5601	0.198	0.2837
C58	0.5628	0.2426	0.2234
C59	0.7596	0.4707	0.2104
C60	0.8032	0.4792	0.245
C61	0.8191	0.521	0.1729
C62	0.7915	0.5535	0.0582
C63	0.7481	0.5449	0.0224
N64	0.861	0.5298	0.2221
N65	0.5179	0.1358	0.4328
N66	0.4342	0.9112	0.74
N67	0.0929	0.5163	0.6956
C68	0.48	0.1165	0.5149
C69	0.478	0.0694	0.5817
C70	0.4386	0.0484	0.6186
C71	0.4368	0.0039	0.68
C72	0.4743	-0.0204	0.708
C73	0.5137	0.0007	0.6723
C74	0.5155	0.0452	0.6093
C75	0.8891	0.4991	0.3383
C76	0.9341	0.5111	0.3991
C77	0.9643	0.48	0.5029
C78	1.0067	0.4918	0.5629
C79	1.0196	0.535	0.521
C80	0.9894	0.566	0.4173
C81	0.9471	0.5541	0.3573
C82	0.8745	0.457	0.4057
C83	0.8315	0.4471	0.3591
C84	0.443	0.1417	0.5356
C85	0.4452	0.1861	0.4754

C86	0.4722	0.9324	0.7666
C87	0.0647	0.5469	0.5807
C88	0.5095	0.9089	0.8399
C89	0.5074	0.8642	0.8821
C90	0.0792	0.5891	0.513
C91	0.1223	0.599	0.5578

Table S3. The chemical composition of NQ-Ni-COF before and after cycling test.

	C (at%)	N (at%)	O (at%)	Ni (at%)
Before	80.81	8.38	10.21	0.60
After	81.13	8.25	10.10	0.51

Table S4. Mass spectrometry piece information and proposed structure of intermediate products in the catalytic degradation of CIP by NQ-Ni-COF.

Intermediate products	ESI (+) MS (*m/z*)	Molecular Formula	Supposed Structure
CIP	332	$C_{17}H_{18}FN_3O_3$	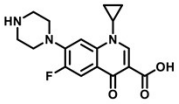
A	330	$C_{17}H_{19}N_3O_4$	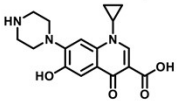
B	359	$C_{17}H_{17}N_3O_6$	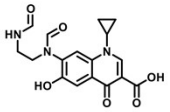
C	306	$C_{15}H_{19}N_3O_4$	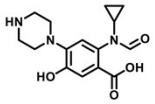
D	212	$C_9H_{13}N_3O_3$	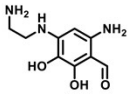
E	362	$C_{17}H_{16}FN_3O_5$	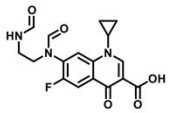
F	334	$C_{16}H_{16}FN_3O_4$	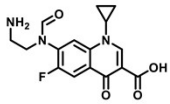
G	306	$C_{15}H_{16}FN_3O_3$	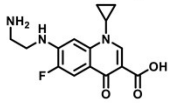
H	318	$C_{16}H_{16}FN_3O_3$	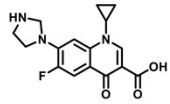
I	290	$C_{15}H_{16}FN_3O_2$	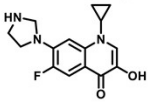
J	274	$C_{15}H_{16}FN_3O$	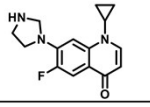

4. Copies of NMR spectra

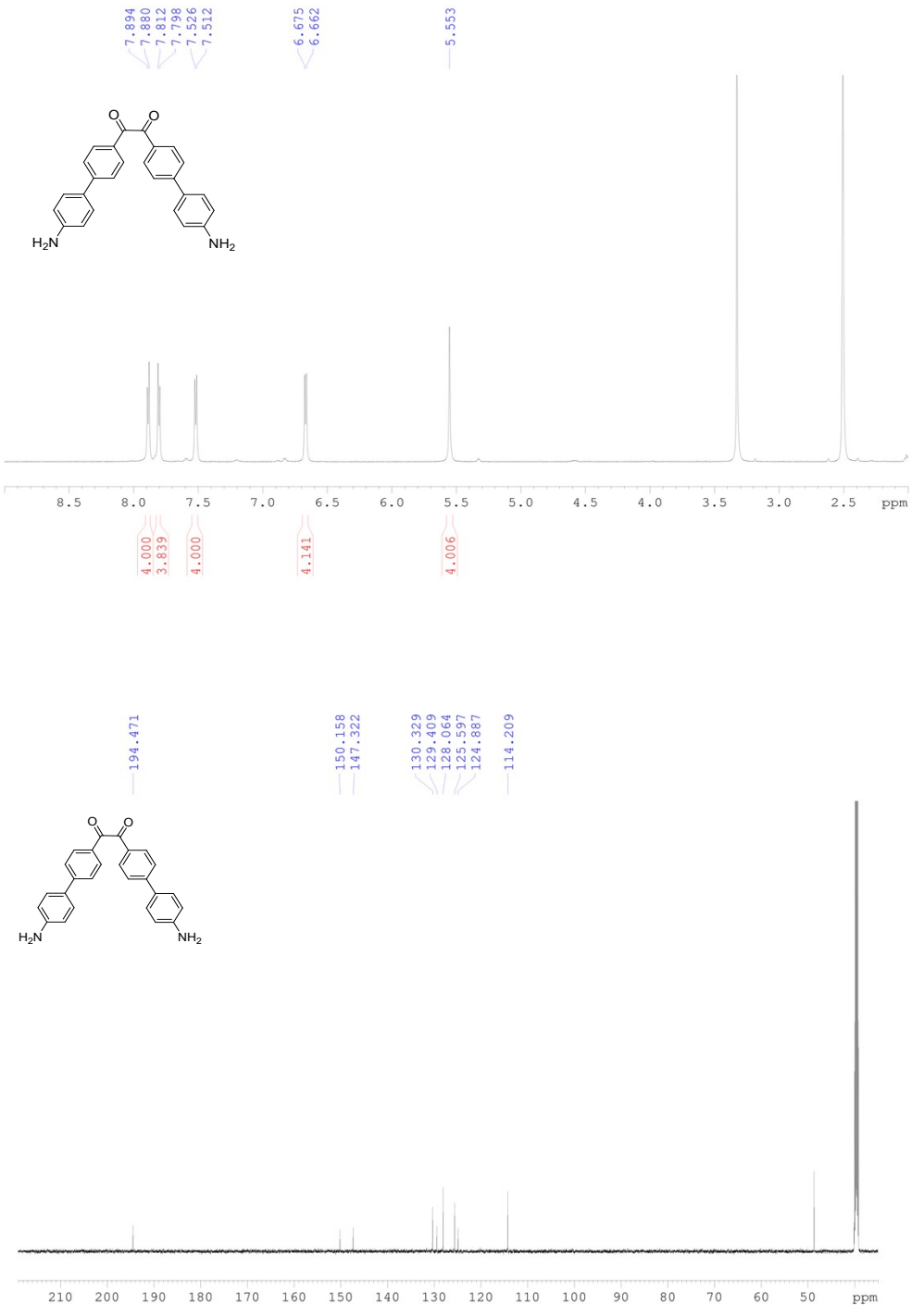

Fig. S14 ^{1}H NMR and ^{13}C NMR spectra of **S3**.

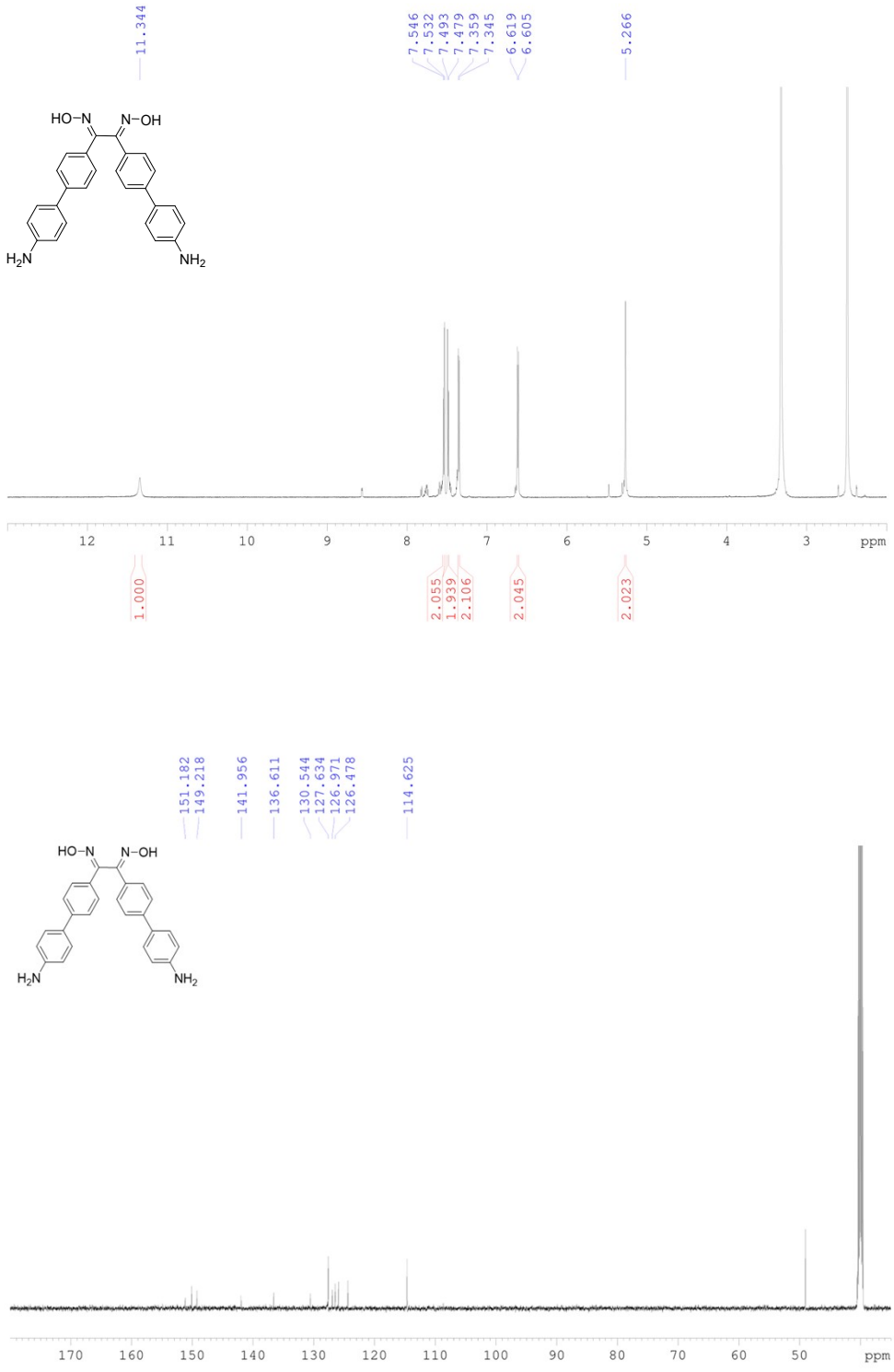

Fig. S15 ^{1}H NMR and ^{13}C NMR spectra of **S4**.

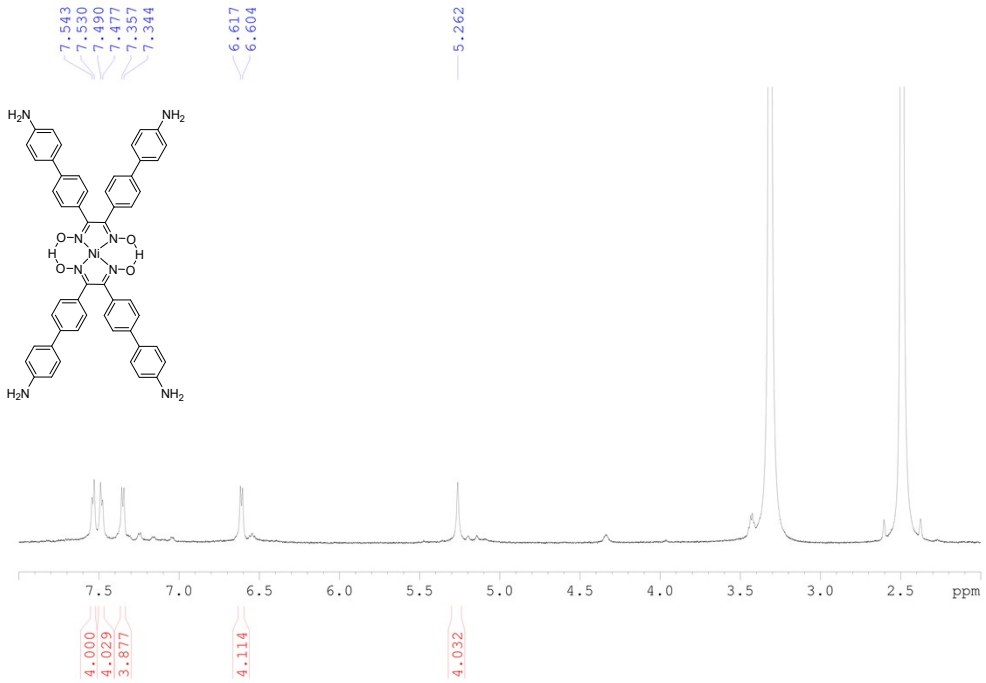

Fig. S16 ^{1}H NMR spectra of **S5**.